Scientia Iranica F (2021) 28(3), 1926–1938

SCIENTIA IRANICA

Sharif University of Technology
Scientia Iranica
Transactions F: Nanotechnology
http://scientiairanica.sharif.edu

Study of thermally developed flow of viscous fluid over a porous stretching surface contacting gyrotatic microorganisms using buongiorno model

Sh. Akhter[a,b] and M. Ashraf [b,*]

a. *Department of Mathematics, COMSATS University Islamabad, Sahiwal 57000, Pakistan.*
b. *Centre for Advanced Studies in Pure and Applied Mathematics (CASPAM), Bahauddin Zakariya University, Multan 60000, Pakistan.*

Received 29 January 2020; received in revised form 15 February 2021; accepted 2 May 2021

KEYWORDS
Bioconvection flow;
Viscous fluid;
Gyrotactic micro-organisms;
Heat generation or absorption;
Porous medium.

Abstract. Recent developments in advanced nanotechnology have given rise to the thermal consequences of nanoparticles due to their increasingly significant roles in different engineering and thermal extrusion systems. In this study, the two-dimensional flow of viscous nanoliquid in the presence of gyrotactic micro-organisms encountered by a porous stretched surface was numerically addressed. The novel aspects of Brownian diffusion and thermophoresis were also studied using Buongiorno model. The effect of thermal radiation was taken into account in the energy equation. Further, a set of pertinent transformations was suggested to transform the governing non-linear partial differential equations into a system of non-linear ordinary differential equations. A well-known numerical method called the finite difference technique was employed to determine the numerical solution of the modeled dimensionless equations. The flow analysis, presented graphically, targeted the effects of numerous prominent parameters on velocity, temperature, concentration, and motile micro-organism profiles. In the presence of thermal radiation, the velocity declined following the increase of bioconvection Rayleigh number and buoyancy ratio parameter value, while an opposite trend was observed when boosting the Grashoff number. The porous medium and radiation increased the fluid temperature.

1. Introduction

Given the inclusive practical applications of nanoparticles in recent decades, considerable attention has been drawn to the study of nanoparticles with physical significance in many industrial, engineering, and real-world problems. The recent development of industrial systems has encouraged researchers to discover new and cheap energy resources. Although numerous traditional techniques have been developed to improve such energy resources and thermal efficiency processes, many environmental problems such as global warming, emission of carbon dioxide, and depletion of ozone layer result from such physical processes. Energy resources based on the utilization of such nanoparticles are suggested as the most fascinating and improved heat transportation mechanisms. Moreover, nanoparticles are also employed in biomedical sciences including lasers, diagnosis of different diseases, annihilation of cancer tissues, brain tumor, artificial lungs, etc.

*. *Corresponding author. Tel.: +92300-7354190*
E-mail addresses: shaheen@cuisahiwal.edu.pk (Sh. Akhter); muhammadashraf@bzu.edu.pk (M. Ashraf)

doi: 10.24200/sci.2021.55209.4178

Further, nanoparticles are also used in engineering processes such as cooling processes, enhancement of extrusion processes, solar systems, etc. Nanoparticles with high thermal conductivity are small-sized solid particles such as carbides (SiC), stable metals (Ag, Al, Cu), and non-metal-like carbon nanotubes and oxides (SiO_2, CuO, and Al_2O_3), all merged in the base fluids such as ethylene glycol, oil, water, and bio-fluids to increase the fluid temperature. The interaction between such enhanced thermo-physical particles was primarily studied by Choi [1] in 1995; however, later on, numerous investigators have shifted their focus onto the flow of small-size particles. For instance, Buongiorno [2] suggested the most significant slip parameters, namely thermophoresis parameter effects, and Brownian motion aspects associated with the movement of nanoparticles. Khan et al. [3] established a series solution for the Maxwell nanofluid configured by a stretched surface with extra effect of heat source/sink and radiative heat flux features. Based on the well-known convergent technique, this series solution was developed by confirming the solution accuracy. Numerical investigation of the natural convection flow of nanoparticles using Lattice Boltzman technique was carried out by Mohebbi et al. [4]. Mashaei et al. [5] performed a numerical simulation to investigate the effects of discrete heat source and sink on the laminar force convection of nanofluid flow across the channel. Kumam et al. [6] employed the homotopic approach to discuss the magnetohydrodynamic and radiative effects in the cross nanofluid associated with rotating channels. Hassan et al. [7] used Forchheimer porous medium model to explore the permeability of nanofluid flow over a wavy surface. Guha and Nayek [8] pointed out the thermal consequences of natural convection flow of nanofluid over a vertical plate. Sheikholeslami et al. [9,10] employed a numerical approach called finite volume method to investigate the increase in the heat transfer rate of nanomaterials. Hakeem et al. [11] reported the thermal features in nanoparticles exposed to permeable configuration. Further recent studies on nanofluid flow can be seen in [12–18].

The practical applications (including crystal growing, extrusion process, glass blowing, and manufacture of foods and papers) of the fluid flow phenomenon over stretching surfaces add up to the significance of their studies. Turkyilmazoglu [19] provided multiple analytical solutions for fluid flows over stretching surfaces. Series solution was employed by Khan [20] to investigate the problem of visco-elastic fluid flow over a stretching sheet. Further recent studies on the applications of fluid flow over stretching surfaces can be seen in [21–27].

In recent years, significant attention has been drawn to the phenomenon of bioconvection due to its numerous applications in modern biotechnology. Bioconvection reveals the microscopic convection of fluid particles associated with the variations in density distribution. The bioconvection process comprises the collective motion of motile microorganisms in some specific directions. Such a self-oriented movement of microorganisms could effectively increase liquid density. Bioconvection occurs when microorganisms that are less dense than water are swimming upward, on average. Different species have different reasons for upward swimming. For example, the oxygen concentration gradient functions as a stimulator, which is responsible for forcing the microorganism to swim in a specific direction by self-propelling. The motion of microorganisms mediated by such stimulators is referred to as taxis, which can be further classified as chemotaxis, phototaxis, gravitaxis, and gyrotaxis. Moreover, the motion of microorganisms that is either towards or away from the light and directed opposite gravity is affected due to chemical gradient and also, towards downwelling due to gravitational viscous effects. To this end, viscous shear forces and gravity effects near the bottom-heavy wall produce torque to control the gyrotaxis. Hence, the bottom-heavy algae/bacteria are involved in bioconvection. The basic difference between the bioconvection and nanofluid indicated that while the bioconvection phenomenon was self-propelled, the movement of nanoparticles was characterized by thermophoresis or Brownian motion. It was experimentally proven that utilization of gyrotactic microorganisms could effectively enhance stability and mass transportation of nanoparticles. Kuznetsov [28,29] primarily investigated the bioconvection phenomenon as well as nanoparticles. Later on, due to the reported significance of this phenomenon in different industries and biotechnology, some researchers have further studied this issue. For instance, Khan et al. [30] conducted a bioconvection study of natural convection fluid flow of nanofluid containing gyrotactic microorganisms passing a truncated cone using convective boundary conditions. Hayat et al. [31] studied the mixed convective flow of viscoelastic nanofluid with gyrotactic microorganisms induced by stretched cylinder. Mehryan et al. [32] numerically presented the thermo-physical characteristics of nanofluid containing the gyrotactic microorganisms configured by nonlinear surface. Akbar [33] inspected the bioconvection phenomenon in the peristaltic transport of nanofluid in the asymmetric channel. Another theoretical bioconvection for micropolar nanofluid was numerically studied by Atif et al. [34]. Zuhra et al. [35] numerically investigated the bioconvection of nanofluid induced by moving plate. Atif et al. [36] also discussed the problem of magnetohydrodynamics Carreau nanofluid over a stretched surface. Nawaz et al. [37] employed a finite element method to discuss the Brownian motion of nanofluid particles subject to hydro-thermal effects.

Further, the latest studies on bioconvection can be seen in [38–40].

The literature review reveals that no study has been conducted on the heat absorption and generation features in thermally developed flow of viscous nanofluid contacting gyrotactic microorganisms over a porous stretching surface through our proposed numerical model. Therefore, the main motivation behind the present study was to fill this gap.

To this end, a mathematical model for the flow, heat, and concentration of a viscous nanofluid over a permeable stretching sheet was developed, taking into account the role of porosity, heat source/sink, and thermal radiation. Moreover, the bioconvection features of nanoparticles were considered in the presence of motile microorganisms. The discretized mathematical equations together with the boundary conditions were numerically treated via an efficient finite difference technique and MATLAB software.

2. Problem statement

Consider a steady, incompressible, and two-dimensional boundary layer nanofluid containing the gyrotactic microorganism induced by a porous stretched and shrunk sheet (Figure 1). Newtonian fluid obeying Boussinesq approximation should also be taken into account. Stretched sheet was assumed to be permeable with suction/injection features. The aspects of thermophoresis and Brownian movement were elaborated using Buongiorno nanofluid. Heat transfer (facilitated by thermal conduction) takes place according to Fourier's Law. Due to the thermally developed surface, the consequence of thermal radiation was considered by Rosseland approximation and heat absorption/generation was also taken into account in the energy equation. It was further assumed that the swimming direction and velocity of the microorganism were not affected by nanoparticles, and the suspension of nanoparticles was assumed to be diluted and stabled. The stretched/shrunk surface

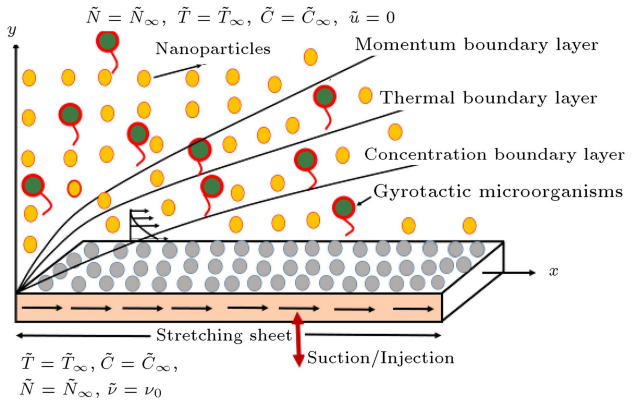

Figure 1. Physical configuration.

was retained by a uniform velocity of $U_w = ax$ where a and x denote the positive constant and coordinate along the stretching/shrinking surface, respectively. The rate of mass transportation (caused by molecular diffusion) can be obtained according to Fick's law with injection ($\nu_o > 0$) and suction ($\nu_o < 0$). Following these assumptions and the studies conducted by Aman et al. [41], Ahmad et al. [42], Sheikholeslami and Rokni [43], and Wahid et al. [44], the author obtained the governing equations in the current flow situation in the following forms:

$$\frac{\partial \tilde{u}}{\partial x} + \frac{\partial \tilde{v}}{\partial y} = 0, \tag{1}$$

$$\tilde{u}\frac{\partial \tilde{u}}{\partial x} + \tilde{v}\frac{\partial \tilde{u}}{\partial y} = \vartheta\frac{\partial^2 \tilde{u}}{\partial y^2} + g\beta\left(1 - \tilde{C}_\infty\right)\left(\tilde{T} - \tilde{T}_\infty\right) - \frac{g}{\rho_f}\left(\rho_p - \rho_f\right)\left(\tilde{C} - \tilde{C}_\infty\right) - \frac{g\gamma}{\rho_f}\left(\rho_m - \rho_f\right)\left(\tilde{N} - \tilde{N}_\infty\right) - \frac{\vartheta}{k^\bullet}\tilde{u}, \tag{2}$$

$$\tilde{u}\frac{\partial \tilde{T}}{\partial x} + \tilde{v}\frac{\partial \tilde{T}}{\partial y} = \left(\alpha + \frac{16\sigma^*\tilde{T}_\infty^3}{3k^*\rho c_p}\right)\frac{\partial^2 \tilde{T}}{\partial y^2} + \frac{Q_0}{\rho c_p}\left(\tilde{T} - \tilde{T}_\infty\right) + \tau\left\{D_B\frac{\partial \tilde{C}}{\partial y}\frac{\partial \tilde{T}}{\partial y} + \frac{D_T}{\tilde{T}_\infty}\left(\frac{\partial \tilde{T}}{\partial y}\right)^2\right\}, \tag{3}$$

$$\tilde{u}\frac{\partial \tilde{C}}{\partial x} + \tilde{v}\frac{\partial \tilde{C}}{\partial y} = D_B\frac{\partial^2 \tilde{C}}{\partial y^2} + \frac{D_T}{\tilde{T}_\infty}\frac{\partial^2 \tilde{T}}{\partial y^2}, \tag{4}$$

$$\tilde{u}\frac{\partial \tilde{N}}{\partial x} + \tilde{v}\frac{\partial \tilde{N}}{\partial y} + \frac{bW_c}{\left(\tilde{C}_w - \tilde{C}_\infty\right)}\left[\frac{\partial}{\partial y}\left(\tilde{N}\frac{\partial \tilde{C}}{\partial y}\right)\right] = D_n\frac{\partial^2 \tilde{N}}{\partial y^2}, \tag{5}$$

where $\tilde{u}$ and $\tilde{\nu}$ represent the horizontal and vertical velocity components, respectively. Further, ϑ, g, $\tilde{T}$, $k^\bullet$, β, α, Q_0, D_B, D_T, D_n, b, W_c, $\tilde{C}$, $\tilde{N}$, τ, ρ_f, ρ_p, c_f, and c_p are the kinematics viscosity, gravity vector, temperature, Darcy permeability, fluid volume expansion coefficient, thermal diffusivity, thermal coefficient, Brownian diffusion coefficient, thermophoresis constant, microorganism diffusivity, chemotaxis constant, maximum cell swimming speed, nanoparticles volume fraction, microorganism concentration, ratio of effective heat capacity of fluid, fluid density, nanoparticles density, and specific heat constant, respectively.

The terms related to bioconvection and porosity are included in the momentum equation. Generally, movements of nanoparticles are stabilized using the microorganisms in the base fluid. Bioconvection has many considerable applications in other fields such as

agriculture, chemistry, biotechnology, and wastewater management. On the contrary, the convective heat and mass transfer in fluid-imbued porous media have an inclusive range of applications including water movements in geothermal reservoirs, thermal insulation engineering, heat pipes, nuclear waste repository, underground spreading of chemical waste, grain storage, geothermal engineering, and higher recovery of petroleum reservoirs. Furthermore, the heat equation is established by the effects of heat source and radiation. Basically, there is a significant temperature difference between the ambient fluid and surface that causes thermal convection with a significant heat sink. There are a number of convection applications in the framework of endothermic and exothermic reactions of chemical compounds. Radiations are utilized in the academic fields of medicine, generating electricity, and industry. Moreover, radiation has other significant applications in archaeology, agriculture, law enforcement, geology, space exploration, and many others.

The appropriate boundary conditions for the considered flow problem are as follows:

$$\tilde{v} = v_0, \quad \tilde{u} = \lambda U_w, \quad \tilde{T} = \tilde{T}_w, \quad \tilde{C} = \tilde{C}_w, \quad \tilde{N} = \tilde{N}_w \quad at \quad y = 0,$$

$$\tilde{u} \to 0, \quad \tilde{T} \to \tilde{T}_\infty, \quad \tilde{C} \to \tilde{C}_\infty, \quad \tilde{N} \to \tilde{N}_\infty \quad as \quad y \to \infty, \tag{6}$$

where λ is the parameter with the stretching of ($\lambda > 0$) and shrinking of ($\lambda < 0$). Moreover, ω and ∞ depict the values on the solid surface far and far away from the surface, respectively.

2.1. Dimensionless quantities

In order to transmute the flow system into a dimensionless form, the following transformations should be taken into account:

$$\psi = (a\vartheta)^{\frac{1}{2}} x f(\eta), \qquad \eta = \left(\frac{a}{\vartheta}\right)^{\frac{1}{2}} y,$$

$$\theta(\eta) = \frac{\tilde{T} - \tilde{T}_\infty}{\tilde{T}_w - \tilde{T}_\infty}, \qquad \phi(\eta) = \frac{\tilde{C} - \tilde{C}_\infty}{\tilde{C}_w - \tilde{C}_\infty},$$

$$\chi(\eta) = \frac{\tilde{N} - \tilde{N}_\infty}{\tilde{N}_w - \tilde{N}_\infty}. \tag{7}$$

Governing Eqs. (2)–(5) were converted into dimensionless forms employing Transformation (7):

$$f''' + ff'' - f'^2 - \varepsilon f' + \mathrm{Gr}(\theta - Nr\phi - Rb\chi) = 0, \tag{8}$$

$$(1 + Rd)\theta'' + \mathrm{Pr}\, f\theta' + \mathrm{Pr}\left(Nb\theta'\phi' + Nt\theta'^2 + \delta\theta\right) = 0, \tag{9}$$

$$\phi'' + \frac{Nt}{Nb}\theta'' + \mathrm{Le} f\phi' = 0, \tag{10}$$

$$\chi'' + Lbf\chi' - \mathrm{Pe}\left[\chi'\phi' + \phi''(\chi + \sigma)\right] = 0, \tag{11}$$

where Continuity Eq. (1) is identically satisfied and it represents the possible fluid motion. Similarly, boundary conditions take the following form:

$$f(0) = S, \quad f'(0) = \lambda, \quad \theta(0) = 1, \quad \phi(0) = 1, \quad \chi(0) = 1,$$

$$f' = 0, \quad \theta = 0, \quad \phi = 0, \quad \chi = 0, \quad as \quad \eta \to \infty, \tag{12}$$

where Gr is the Grashoff number, Nr the buoyancy number, Rb the bioconvection Rayleigh number, ε the porosity parameter, Pr the Prandtl number, Nb the Brownian motion, Nt the thermophoresis parameter, δ the source/sink parameter, Le the Lewis number, Lb the bioconvection Lewis number, σ the dimensionless parameter, Pe the bioconvection Peclet number, and S the mass flux parameter with the suction of ($S > 0$) and injection of ($S < 0$). Mathematically, these parameters are expressed as follows:

$$\mathrm{Gr} = \frac{g\beta\left(1 - \tilde{C}_\infty\right)\left(\tilde{T}_w - \tilde{T}_\infty\right)}{a\tilde{u}},$$

$$Nr = \frac{(\rho_p - \rho_f)\left(\tilde{C}_w - \tilde{C}_\infty\right)}{\beta\rho_f\left(1 - \tilde{C}_\infty\right)\left(\tilde{T}_w - \tilde{T}_\infty\right)},$$

$$Rb = \frac{\gamma(\rho_m - \rho_f)\left(\tilde{N}_w - \tilde{N}_\infty\right)}{\beta\rho_f\left(1 - \tilde{C}_\infty\right)\left(\tilde{T}_w - \tilde{T}_\infty\right)},$$

$$Nb = \frac{\tau D_B\left(\tilde{C}_w - \tilde{C}_\infty\right)}{\vartheta}, \qquad Nt = \frac{\tau D_t\left(\tilde{T}_w - \tilde{T}_\infty\right)}{\vartheta\tilde{T}_\infty},$$

$$\delta = \frac{Q_0}{a\rho c_f}, \qquad \mathrm{Le} = \frac{\vartheta}{D_B}, \qquad \mathrm{Pr} = \frac{\vartheta}{\alpha},$$

$$\varepsilon = \frac{\vartheta}{ak^\bullet}, \qquad Lb = \frac{\vartheta}{D_n}, \qquad \sigma = \frac{\tilde{N}_\infty}{\tilde{N}_w - \tilde{N}_\infty},$$

$$\mathrm{Pe} = \frac{bW_c}{D_n}.$$

2.2. Physical quantities

In the present study, the physical quantities of practical interest include the skin friction coefficient, local Nusselt number, local Sherwood number, and local density of motile microorganisms, justified in the following forms:

$$C_f = \frac{\tau_w}{\rho U_w^2}, \qquad \mathrm{Nu}_x = \frac{xq_w}{k\left(\tilde{T}_w - \tilde{T}_\infty\right)},$$

$$\mathrm{Sh}_x = \frac{xq_m}{D_B\left(\tilde{C}_w - \tilde{C}_\infty\right)}, \qquad \tau_w = \mu\left(\frac{\partial\tilde{u}}{\partial y}\right)_{y=0},$$

$$q_w = -k\left(\frac{\partial \tilde{T}}{\partial y}\right)_{y=0}, \qquad q_m = -D_B\left(\frac{\partial \tilde{C}}{\partial y}\right)_{y=0},$$

$$q_n = -D_n\left(\frac{\partial \tilde{N}}{\partial y}\right)_{y=0}, \tag{13}$$

where τ_w, q_w, q_m, and q_n are surface shear stress, wall heat flux, wall mass flux, and motile microorganism's density, respectively.

The physical quantities defined in Eq. (13) may be written as:

$$C_f \mathrm{Re}_x^{-1/2} = f''(0), \quad \mathrm{Nu}_x \mathrm{Re}_x^{-1/2} = -\theta'(0),$$

$$\mathrm{Sh}_x \mathrm{Re}_x^{-1/2} = -\phi'(0), \quad Nn_x \mathrm{Re}_x^{-1/2} = -\chi'(0), \tag{14}$$

where $\mathrm{Re}_x = U_w x/\vartheta$ is the local Reynolds number.

3. Numerical solution

Mathematicians, scientists, and researchers have shifted their focus to solving nonlinear physical models since most of the nonlinear physical models already exist in nature. Some researchers, namely Wahid et al. [45,46], Turkyilmazoglu [47], and Khan et al. [48], suggested analytical solutions for such physical phenomena under certain conditions. The governing equations of the present physical model are highly nonlinear; therefore, it is difficult to solve such differential equations analytically. In this regard, a numerical technique known as finite difference method was employed in this study to solve such nonlinear coupled equations. As Eq. (8) is of the 3rd order, firstly, we reduced its order by substituting $f'(q)$. Hence, the equations and their corresponding boundary conditions take the following form:

$$q'' + fq' - q^2 - \varepsilon q = \mathrm{Gr}\left(Nr\phi + Rb\chi - \theta\right), \tag{15}$$

$$(1+Rd)\,\theta'' + \mathrm{Pr}\, f\theta' = -\mathrm{Pr}\left(Nb\theta'\phi' + Nt\theta'^2 + \delta\theta\right), \tag{16}$$

$$\phi'' + \mathrm{Le} f\phi' = -\frac{Nt}{Nb}\theta'', \tag{17}$$

$$\chi'' + (Lbf - \mathrm{Pe}\phi')\,\chi' - \mathrm{Pe}\chi\phi'' = \mathrm{Pe}\sigma\phi''. \tag{18}$$

The corresponding boundary conditions take the following form:

$$f(0) = S, \ q(0) = \lambda, \ \theta(0) = 1, \ \phi(0) = 1, \ \chi(0) = 1,$$

$$q = 0, \quad \theta = 0, \quad \phi = 0, \quad \chi = 0, \quad as \quad \eta \to \infty. \tag{19}$$

To perform the numerical computation for the above-formulated equations, the flow domain $[0, \infty)$ with the step size of h was first discretized. Famous Simpson's numerical iterative procedure was then used to integrate the equation $f' = q$. Further, central difference approximation was employed to discretize the involved derivatives in Eqs. (15)–(19) and then, the iterative solution was obtained using Succession Over Relaxation (SOR) method. This iterative method stops functioning when

$$\max\Big(||q_{i+1} - q_i||_2, ||f_{i+1} - f_i||_2, ||\theta_{i+1} - \theta_i||_2,$$

$$||\phi_{i+1} - \phi_i||_2, ||\chi_{i+1} - \chi_i||_2\Big) < Tol_{itr},$$

is satisfied up to four consecutive iterations.

4. Results and discussion

In this section, the effects of the involved physical parameters on the velocity, temperature, concentration, and motile microorganism distributions are discussed. These parameters are characterized by material and flow properties, all with the geometric dimensions. Instead of allocating specific domain dimensions and fluid properties to these parameters, a better approach is allocating fixed values to these parameters in order to analyze the flow and thermal characteristics of fluid dynamics problems (as stated by Ahmad et al. [42] and Wahid et al. [44]). The range of parameters in this study was chosen such that a further increment in the upper limit would not affect the qualitative behavior of the profiles. Figures 2–18 present a detailed discussion of the obtained numerical results describing the effects of different governing parameters such as traditional Lewis number Le, bioconvection Lewis number Lb, bioconvection Péclet number Pe, suction/injection parameter S, bioconvection Rayleigh number Rb, buoyancy ratio parameter Nr, Brownian

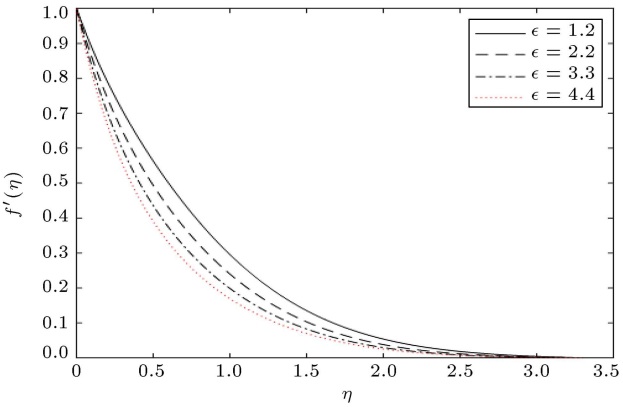

Figure 2. The variation in velocity for $S = 0.2$, $\mathrm{Gr} = 5$, $Nr = 0.4$, $Rb = 0.6$, $\mathrm{Pr} = 4.5$, $Nb = Nt = \sigma = \delta = 0.1$, $\mathrm{Le} = 4.5$, $\mathrm{Pe} = 1.2$, $Lb = 0.9$, $Rd = 0.9$, $\lambda = 1$, and various ε.

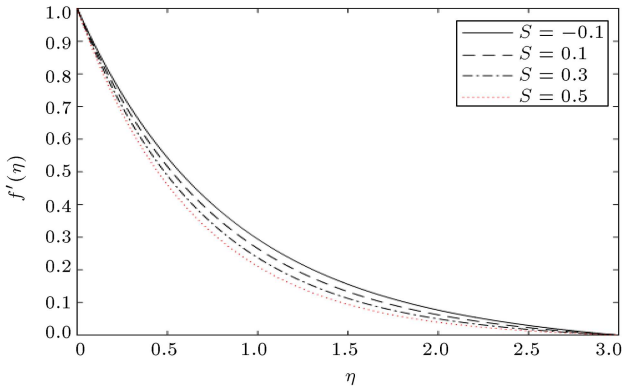

Figure 3. The variation in velocity for $\varepsilon = 0.7$, $Nr = Rb = 0.2$, Pr = 3.2, Gr $= Nb = Nt = \sigma = \delta = 0.1$, Le = 4.9, Pe = 0.9, $Lb = 1.2$, $Rd = 0.9$, $\lambda = 1$, and different S.

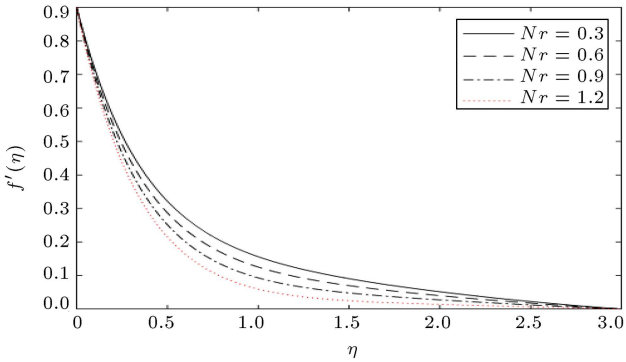

Figure 4. The variation in velocity for $S = Rb = Nb = Nt = Lb = 0.2$, $\varepsilon = 6$, Gr = 1.8, Pr = 2.5, $\sigma = \delta = 0.1$, Le = 1.6, Pe = 2, $Rd = 2.3$, $\lambda = 0.9$, and various Nr.

motion parameter Nb, thermophoresis parameter Nt, permeability parameter ε, Grashof number Gr, Prandtl number Pr, microorganisms concentration difference parameter χ, heat source/sink parameter δ, and dimensionless parameter σ.

The effects of buoyancy ratio Nr, permeability parameter ε, mixed convection Gr, bioconvected Rayleigh number Rb, and suction/injection parameter S on velocity are shown in Figures 2–6. Based on the velocity profiles in the mentioned figures, it can be concluded that while the velocity was maximum on the plate surface, it was exponentially reduced to zero in the region beyond the plate surface at the free stream.

Figure 2 shows the effects of porosity parameter ε on the velocity field $f'(\eta)$. Upon increasing the porosity of the medium, the velocity field would decrease. Such a declining trend can be justified based on the sizes of pores inside the porous medium which become larger. In this case, a resistive force from the opposite direction of the flow was imposed on the fluid and consequently, the velocity boundary layer thickness was reduced. The effect of suction/injection parameter S on the velocity distribution $f'(\eta)$ is shown

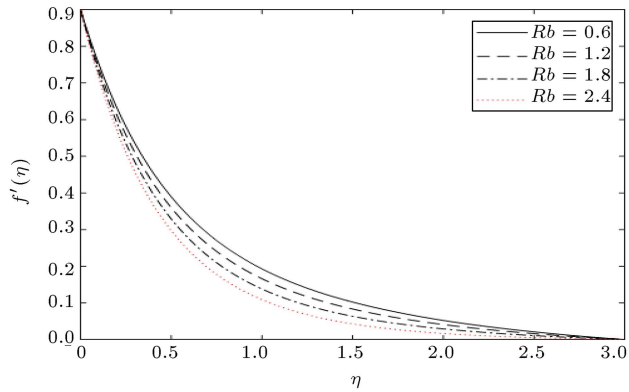

Figure 5. The variation in velocity for $S = 0.1$, $\varepsilon = 3$, Gr $= \lambda = 0.9$, $Nr = 0.2$, $Nb = Nt = Lb = 0.3$, Pr = 2, $\sigma = \delta = 0.1$, Le = 4.9, Pe = 1.1, $Rd = 0.8$, and various Rb.

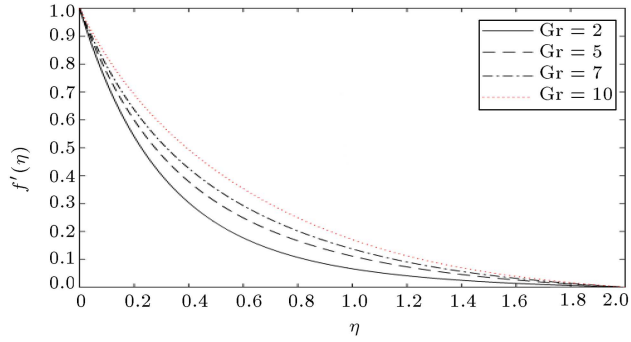

Figure 6. The variation in velocity for $S = Rb = \sigma = 0.3$, $\varepsilon =$ Pr $= 10$, $Nr = Nb = Nt = \delta = 0.1$, Le = 5.5, Pe = 0.5, $Lb = 0.9$, $Rd = 3.5$, $\lambda = 1$, and various Gr.

in Figure 3. The visualized results showed a gradual decrease in $f'(\eta)$. Physically, the escalating behavior of dragging the nanofluid particles through the stretching surface was observed upon increase in the value of the suction parameter S, which decreased the velocity profile. As observed in Figure 4, a declining velocity profile was already predicted by Nr evaluation. In fact, resistive buoyancy forces (functioning opposite to the pressure gradient) resulted from strengthening Nr, which reduced the fluid flow speed. The effect of Rayleigh number Rb on the velocity $f'(\eta)$ is shown in Figure 5. According to this figure, it was predicted that the velocity profile would decrease upon increasing the Rayleigh number. The physical features of the above occurrence involve the bioconvection Rayleigh number Rb which includes the buoyancy ratio (resistive) forces, which are responsible for resisting the movement of fluid particles in the entire flow domain. Physically, the effects of buoyancy forces were intensified upon increasing the values of Rb, leading to the fluid velocity decline. On the contrary, the opposite trend was observed for Gr, as can be seen in Figure 6. Of note, the fluid velocity $f'(\eta)$ increased following an increase in the Grashoff number Gr, which was related to the involvement of buoyancy ratio forces versus viscous

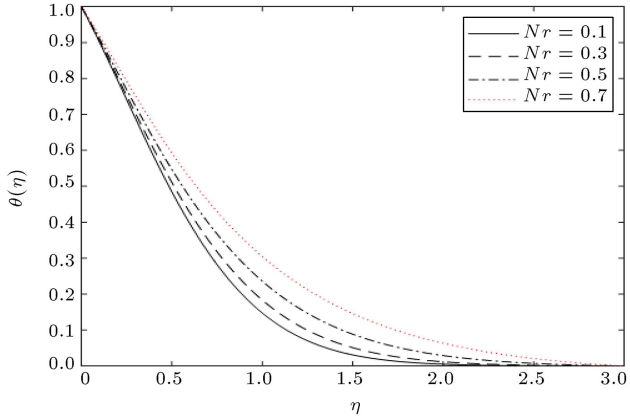

Figure 7. The variation in temperature for $S = 0.3$, $\varepsilon = 6$, Gr $= 5.8$, $Rb = \sigma = 0.2$, Pr $= 6.8$, $Nb = Nt = Rd = 0.3$, $Lb = 1.5$, $\delta = 0.1$, Le $=$ Pe $= 2$, $\lambda = 1$, and various Nr.

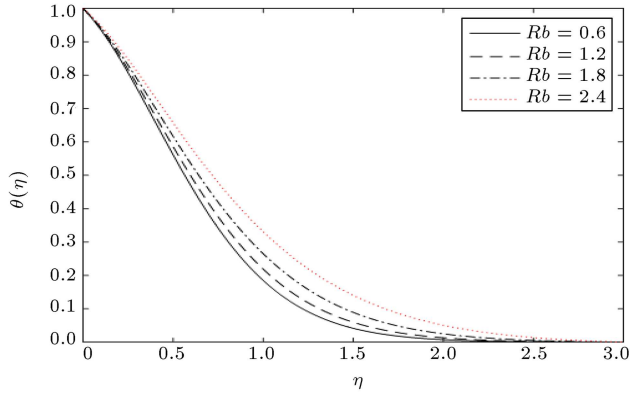

Figure 8. The variation in temperature for $S = 0.3$, $\varepsilon = 6$, Gr $= 4$, $Nr = Rd = 0.2$, Pr $= 6$, $Nb = Nt = 0.3$, $Lb = 1.3$, $\sigma = \delta = 0.1$, Le $= 4.9$, Pe $= 1.2$, $\lambda = 1$, and various Rb.

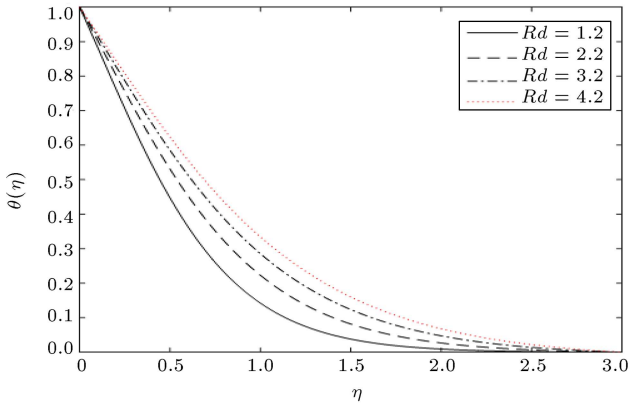

Figure 9. The variation in temperature for $S = Nr = \sigma = 0.2$, $\varepsilon =$ Le $= 5.5$, Gr $= 4$, $Rb = 0.4$, Pr $= 10$, $Nb = Nt = \delta = 0.1$, $Lb = 0.8$, Pe $= 1.3$, $\lambda = 1$, and various Rd.

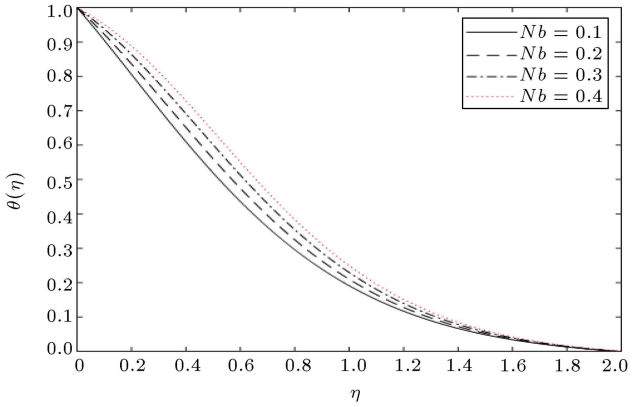

Figure 10. The variation in temperature for $S = 0.2$, $\varepsilon = 4$, Gr $= 5$, $Nr = 0.4$, $Rb = 0.3$, Pr $= 7$, $Rd = 0.9$, $Nt = Lb =$ Pe $= \sigma = \delta = 0.1$, Le $= 5.5$, $\lambda = 1$, and various Nb.

forces. Increasing the Grashoff number may weaken the effect of viscous forces, which augment the fluid velocity.

The graphical consequences for buoyancy ratio parameter Nr bioconvection Rayleigh number Rb radiation parameter Rd Brownian motion parameter Nb, thermophoresis parameter Nt, and heat source/sink parameter δ on the temperature $\theta(\eta)$ are given in Figures 7–12. According to Figures 7 and 8, the temperature of the nanofluid increases following an increase in both bioconvection Rayleigh number Rb and buoyancy ratio parameter Nr. The physical aspect of strengthening the temperature profiles is related to the involvement of the buoyancy forces. The effect of radiation parameter Rd on the temperature is illustrated in Figure 9. Upon increasing the radiation parameter, the temperature profiles would rise. Physically, in case the radiation parameter increased, the mean absorption coefficient would decrease, thus increasing the rate of the radiative heat transfer to the liquid. Consequently, the temperature of the fluid would increase. The behavioral effects of Nb and Nt on $\theta(\eta)$ are depicted in Figures 10 and 11. It was predicted that the thickness and temperature of the thermal boundary layer would be the increasing functions of Nb and Nt. Random motion of fluid particles was escalated by increasing Nb, as a result of which considerable heat was produced, thus increasing the temperature of the fluid. On the contrary, due to thermophoresis, a large number of nanoparticles were pulled away from the hot to cold surface, thus increasing the temperature of the fluid.

The effects of heat source/sink parameter δ on temperature distribution are elaborated in Figure 12, indicating that any increase in the temperature resulted from an increase in the heat source strength. Moreover, by increasing the heat source strength, a considerable amount of heat entered the system; hence, the temperature of the fluid increased and thermal boundary layer thickness increased. This result was of significance in the heat transfer flow problems.

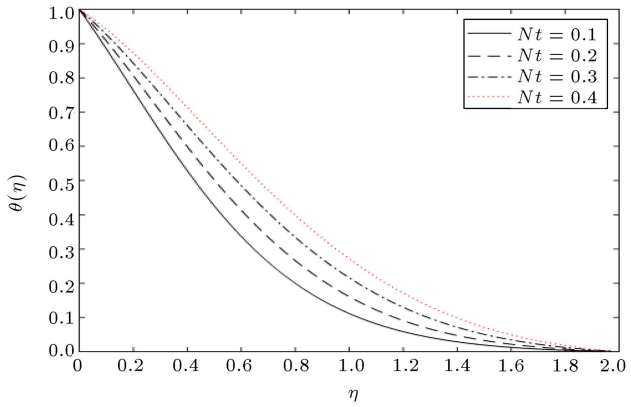

Figure 11. The variation in temperature for $S = Nb = \sigma = Rd = Lb = \delta = 0.1$, $\varepsilon = \text{Le} = 4.5$, $\text{Gr} = 3.5$, $Nr = 0.2$, $Rb = 0.3$, $\text{Pr} = 7.5$, $\text{Pe} = 1.1$, $\lambda = 1$, and various Nt.

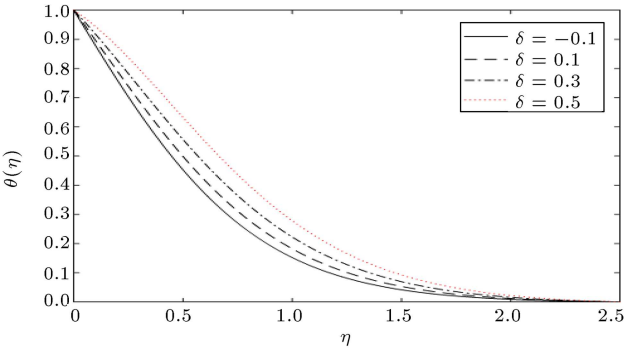

Figure 12. The variation in temperature profiles for $Nt = Nb = \sigma = 0.1$, $S = Nr = Rb = 0.2$, $\varepsilon = 0.7$, $\text{Gr} = 1.7$, $\text{Pr} = 5.2$, $\text{Le} = 4.9$, $\text{Pe} = Rd = 0.9$, $Lb = 1.2$, $\lambda = 1$, and various δ.

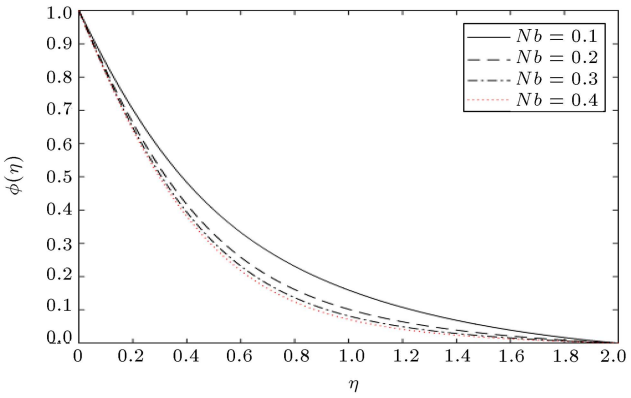

Figure 13. The variation in concentration for $S = Nr = Rb = Nt = Lb = \sigma = \delta = 0.1$, $\varepsilon = 4.5$, $\text{Gr} = 4$, $\text{Pr} = 7.5$, $\text{Le} = 5.5$, $\text{Pe} = 1.1$, $Rd = 2.2$, $\lambda = 1$, and various Nb.

Figure 13 shows the effects of Brownian motion parameter Nb on the concentration profiles. The particles frequently collided with each other following an increase in Nb. Hence, concentration profiles decreased with an increase in Nb. The effect of thermophoresis

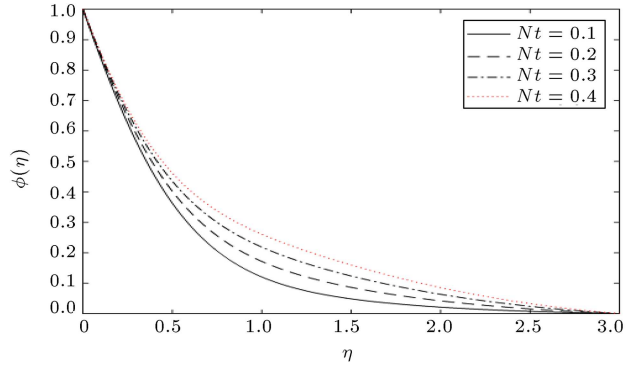

Figure 14. The variation in concentration for $S = Rb = Nr = \delta = \text{Pe} = Rd = Lb = 0.1$, $\varepsilon = \text{Gr} = \text{Le} = 4.5$, $\text{Pr} = 1.5$, $Nb = 0.2$, $\sigma = 0.3$, $\lambda = 1$, and various Nt.

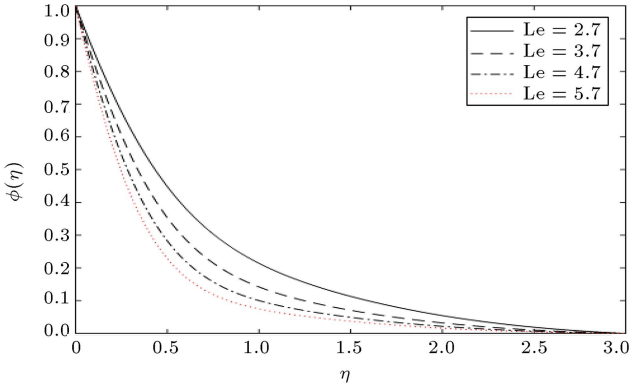

Figure 15. The variation in concentration for $S = Lb = 0.2$, $\varepsilon = 4$, $\text{Gr} = 3$, $Nr = \delta = 0.1$, $Rb = \sigma = 0.3$, $\text{Pr} = 9$, $Nb = 0.9$, $Nt = 0.4$, $\text{Pe} = 1.3$, $Rd = 3.2$, $\lambda = 1$, and various Le.

parameter Nt on the concentration profile is shown in Figure 14. Of note, concentration profiles are the increasing function of Nt. An increase in Nt can enhance the thermal conductivity of the fluid, which is responsible for the enhancement of the concentration profiles. Figure 15 is designed to examine the effect of Lewis number Le on the concentration. It can be observed that the concentration boundary layer thickness and concentration profiles decreased upon increasing the values of Lewis number Le. Given that Brownian diffusion coefficient is inversely proportional to the Lewis number, low diffusivity occurs at larger values of Lewis number Le. Therefore, concentration distributions decreased by increasing the Lewis number Le. The effect of the Peclet number Pe on the motile density profiles is shown in Figure 16. An increase in Pe would decrease the diffusivity of microorganisms, thus decreasing the motile density of the fluid. The effects of microorganism concentration parameter and bioconvection Lewis number on motile density are presented in Figures 17 and 18. Moreover, deterioration in motile density would be observed by increasing the microorganism concentration difference parameter and

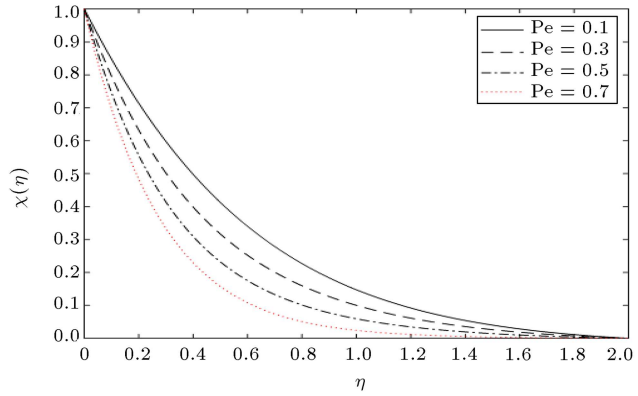

Figure 16. The variation in density of motile microorganism for $S = 0.3$, $\varepsilon = 1.5$, Gr = 2, $Nr = Nt = Rb = 0.1$, Pr $= \sigma = 0.5$, $Nb = 1.3$, $\delta = 0.7$, Le = 4.5, $Lb = 1.8$, $Rd = 0.2$, $\lambda = 1$, and various Pe.

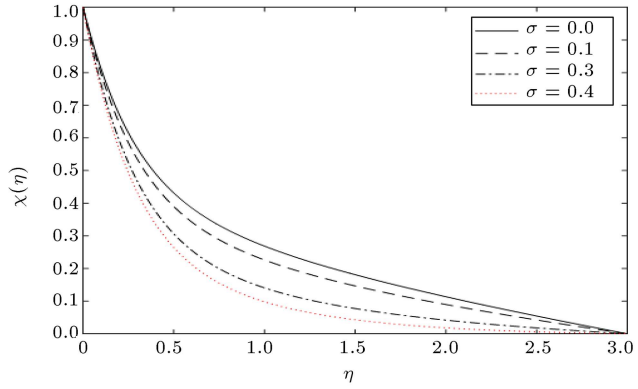

Figure 17. The variation in density of motile microorganism for $S = 0.2$, $\varepsilon = 3$, Gr = 4, $Rb = 0.4$, Pr = 3.5, $Nr = Nb = Nt = Lb = \delta = 0.1$, Le = 4.5, Pe $= Rd = 1.2$, $\lambda = 1$, and various σ.

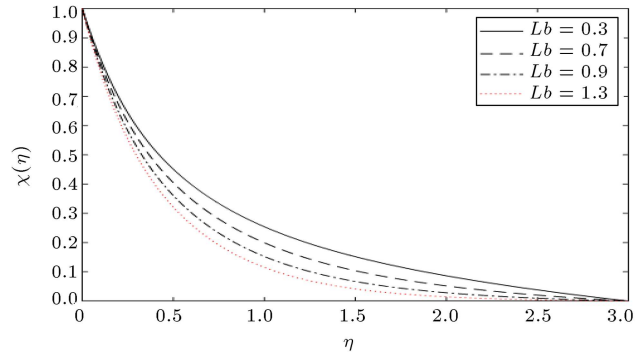

Figure 18. The variation in density of motile microorganism for $S = Nr = Rb = 0.2$, $\varepsilon = 0.7$, $Nt = Nb = \sigma = 0.1$, Gr = 1.7, Pr = 5.2, Le = 4.9, Pe $= Rd = 0.9$, $\delta = 1.2$, $\lambda = 1$, and different Lb.

bioconvection Lewis number. Physically, following an increase in σ, the surface concentration would decrease, hence decay in the strength of particles and mass reduction. Consequently, a decrement in density profiles occurs. Furthermore, an increase in Lb may reduce the microorganism diffusivity, which is responsible for the reduction in the motile density of microorganisms.

Table 1. The comparison values of $-\theta'(0)$, $(Rd = \delta = \text{Gr} = Rb = Nr = \varepsilon = M = 0)$ with those in [41].

λ	$-\theta'(0)$	
	Literature results [41]	**Present results**
1.0	3.4822	3.4849
1.6	3.4589	3.4584
2.0	3.4415	3.4417

Table 2. Variations in $f''(0)$ for different values of Gr, Nr, Rb, and ε when $S = 1$, and $Nt = 0.1$, Pr = 0.7, $Rd = 0.5$, $\sigma = \delta = 0.2$, $Nb = 0.7$, Le = 0.2, Pe = 1.3, $Lb = 0.3$, and $\lambda = 1$ are fixed.

Gr	Nr	Rb	ε	$f''(0)$
0.2	0.5	0.3	0.5	−1.79089
0.5				−1.74615
0.9				−1.68902
0.2	0.1	0.3	0.5	−1.2706
	0.3			−1.75780
	0.5			−1.79034
0.2	0.5	0.2	0.5	−1.78009
		0.3		−1.79147
		0.4		−1.80126
0.2	0.5	0.3	0.3	−1.71210
			0.6	−1.82920
			0.9	−1.93532

Table 1 illustrates a comparison of the values of $-\theta'(0)$ with those reported by Aman et al. [41] through neglecting the existence of the effects of porosity parameter, radiation parameter, mixed convection, magnetic field, and heat absorption/generation parameters in Eqs. (9) and (10). The results of this comparison are in excellent agreement with the numerical results, thus ensuring their accuracy.

The effects of different parameters such as Gr, Nr, Rb, and ε on $f''(0)$ are illustrated in Table 2, according to which $f''(0)$ increased upon increasing Nr, Rb, and ε in contrast to Gr. Table 3 presents the numerical variations of $-\theta'(0)$ against various parameters Nr, Rb, Nb, Nt, Rd, Pr, and δ. As observed, the local Nusselt number $-\theta'(0)$ had the maximum values in terms of δ and Pr; however, an opposite trend was observed for other ones. The effect of different values of Nr, Rb, Nb, Nt, and Le on $-\phi'(0)$ is shown in Table 4. While the local Sherwood number $-\phi'(0)$ would increase by increasing Nb and Le, an opposite trend was observed

Table 3. Variations in $-\theta'(0)$ versus different values of Nt, Nr, Rb, Pr, Rd, δ, and Nb when $S = 1$, $\varepsilon = 0.5$, Gr $= 0.2$, $\sigma = 0.2$, Le $= 0.2$, Pe $= 1.3$, $Lb = 0.3$, and $\lambda = 1$ are fixed.

Nt	Nr	Rb	Pr	Rd	δ	Nb	$-\theta'(0)$
0.2	0.5	0.3	0.7	0.5	0.2	0.7	0.50936
0.4							0.47009
0.6							0.44871
0.2	0.1	0.3	0.7	0.5	0.2	0.7	0.52374
	0.3						0.50390
	0.5						0.50054
0.2	0.5	0.2	0.7	0.5	0.2	0.7	0.51994
		0.3					0.50020
		0.4					0.49908
0.2	0.5	0.3	0.1	0.5	0.2	0.7	0.31895
			0.3				0.33285
			0.4				0.36539
0.2	0.5	0.3	0.7	0.2	0.2	0.7	0.59400
				0.4			0.52601
				0.6			0.48298
0.2	0.5	0.3	0.7	0.5	0.1	0.7	0.33087
					0.3		0.46379
					0.5		0.68111
0.2	0.5	0.3	0.7	0.5	0.2	0.3	0.56775
						0.5	0.52642
						0.7	0.50328

for other parameters. Finally, Table 5 presents the numerical variations of $-\chi'(0)$ against values of Nr, Rb, Pe, and Lb. A careful observation of this table revealed that while motile density of microorganisms decreased following increase in Nr and Rb, it increased by taking into account the effects of Pe and Lb. Of note, multiple solutions may be available for the shrinking of the sheet and suction (as stated by Turkyilmazoglu [19], Lund et al. [49], and Mustafa et al. [50]) which can be further studied and presented in a subsequent paper.

5. Conclusions

The main objective of the present study was to investigate the bioconvection aspects in the flow, heat, and concentration of nanofluid over a porous trenched

Table 4. Variations in $-\phi'(0)$ for different values of Nr, Rb, Nb, Nt, and Le when $S = 1$, $\varepsilon = 0.5$, Gr $= 0.2$, Pr $= 0.7$, $Rd = 0.5$, $\sigma = \delta = 0.2$, Pe $= 1.3$, $Lb = 0.3$, and $\lambda = 1$ are fixed.

Nr	Rb	Le	Nb	Nt	$-\phi'(0)$
0.1	0.3	0.2	0.7	0.1	0.41332
0.3					0.38247
0.5					0.37919
0.5	0.2	0.2	0.7	0.1	0.41244
	0.3				0.38168
	0.4				0.38013
0.5	0.3	0.1	0.7		0.33087
		0.2		0.1	0.37071
		0.4			0.56651
0.5	0.3	0.2	0.3	0.1	0.34443
			0.5		0.35571
			0.7		0.37117
0.5	0.3	0.2	0.7	0.2	0.37689
				0.4	0.28294
				0.6	0.22644

Table 5. Variations in $-\chi'(0)$ for different values of Nr, Rb, Pe, and Lb when $S = 1$, $\varepsilon = 0.5$, Gr $= 0.2$, $Nt = 0.1$, Pr $= 0.7$, $Rd = 0.5$, $\sigma = \delta = 0.2$, $Nb = 0.7$, Le $= 0.2$, and $\lambda = 1$ are fixed.

Nr	Rb	Pe	Lb	$-\chi'(0)$
0.1	0.3	1.3	0.3	1.03634
0.3				0.98854
0.5				0.98207
0.5	0.2	1.3	0.3	1.03285
	0.3			0.98546
	0.4			0.98273
0.5	0.3	0.1	0.3	0.57577
		0.4		0.64800
		0.7		0.75010
0.5	0.3	1.3	0.2	0.92035
			0.5	1.21521
			0.7	1.45375

configuration embedded in a resistive porous medium. The obtained numerical results were evaluated using an efficient method based on finite difference scheme. This method could provide fast convergence. The major observations are listed in the following:

- The porosity of the medium and suction through the sheet slowed the flow velocity;

- The temperature of nanoparticles increased upon applying proper variations to both thermophoresis and Brownian motion constants;
- The heat transfer rate increased following an increase in the Prandtl number;
- The variation in Lewis number decreased the concentration;
- The Peclet and bioconvection Rayleigh numbers decreased the distribution of gyrotactic microorganisms;
- The porous medium increased the fluid temperature.

A comparison of the obtained results in this study with those from [41] showed that the resistive forces of the porous medium and thermal radiations were more capable to handle the bioconvection flows with greater shear stresses and higher temperatures in comparison to the flows over a stretching sheet embedded in a non-porous medium without radiation. The reported results may be helpful in the bio-fuels applications and thermal extrusion phenomenon.

Acknowledgements

The authors would like to express their sincere gratitude to the reviewers and the editor for their careful reading and helpful remarks which helped enhanced the overall quality of this paper.

References

1. Choi, S.U.S. "Enhancing thermal conductivity of fluids with nanoparticles", *ASME Pub. Fed.*, **231**, pp. 99–106 (1995).
2. Buongiorno, J. "Convective transport in nanofluids", *J. Heat Transfer*, **128**, pp. 240–250 (2006).
3. Khan, M., Irfan, M., and Khan, W.A. "Impact of heat source/sink on radiative heat transfer to Maxwell nanofluid subject to revised mass flux condition", *Results Phys.*, **9**, pp. 851–857 (2018).
4. Mohebbi, R., Izadi, M., and Chamkha, A.J. "Heat source location and natural convection in a C-shaped enclosure saturated by a nanofluid", *Phys. Fluids*, **29**(12), 1222009(1–13) (2017). DOI: 10.1063/1.4993866
5. Mashaei, P.R., Hosseinalipour, S.M., and Bahiraei, M. "Numerical investigation of nanofluid forced convection in channels with discrete heat sources", *J. Appl. Math*, **2012**, 259284(1–18) (2012). DOI: 10.1155/2012/259284
6. Kumam P., Shah, Z., Dawar, A., et al. "Entropy generation in MHD radiative flow of CNTs Casson nanofluid in rotating channels with heat source/sink", *Math Probl. Eng.*, 9158093(1–14) (2019). DOI: 10.1155/2019/9158093
7. Hassan, M., Marin, M., Alsharif, A., et al. "Convective heat transfer flow of nanofluid in a porous medium over wavy surface", *Phys. Lett. A*, **382**(38), pp. 2749–2753 (2018).
8. Guha, A. and Nayek, S. "Thermo-fluid-dynamics of natural convection around a heated vertical plate with a critical assessment of the standard similarity theory", *Phys. Fluids*, **29**(10), 103607(1–17) (2017). DOI: 10.1063/1.4990279
9. Sheikholeslami, M., Jafaryar, M., Said, Z., et al. "Modification for helical turbulator to augment heat transfer behavior of nanomaterial via numerical approach", *Appl. Therm. Eng.*, **182**, 115935(1–18) (2020). DOI: 10.1016/j.applthermaleng.2020.115935
10. Sheikholeslami, M., Farshad, S.A., Shafee, A., et al. "Performance of solar collector with turbulator involving nanomaterial turbulent regime", *Renew. Energy*, **163**, pp. 1222–1237 (2020).
11. Hakeem, A.K.A., Indumathi, N., Ganga, B., et al. "Comparison of disparate solid volume fraction ratio of hybrid nanofluids flow over a permeable flat surface with aligned magnetic field and Marangoni convection", *Sci. Iran.*, **27**(6), pp. 3367–3380 (2020). DOI: 10.24200/SCI.2020.51681.2312
12. Turkyilmazoglu, M. "Single phase nanofluids in fluid mechanics and their hydrodynamic linear stability analysis", *Comput. Meth. Prog. Bio.*, **187**, 105171(1–39) (2020). DOI: 10.1016/j.cmpb.2019.105171
13. Sadeghi, V., Baheri, S., and Arsalani, N. "An experimental investigation of the effect of using non-Newtonian nanofluid- graphene oxide /aqueous solution of sodium carboxymethyl cellulose- on the performance of direct absorption solar collector", *Sci. Iran.* (2020). (In Press)
DOI: 10.24200/SCI.2020.54994.4024
14. Sheikholeslami, M., Rizwan-ul Haq, Ahmad, S., et al. "Heat transfer simulation of heat storage unit with nanoparticles and fins through a heat exchanger", *Int. J. Heat Mass Transf.*, **135**, pp. 470–478 (2019).
15. Sheikholeslami, M., Behnoush, R., Milad, D., et al. "Application of nano-refrigerant for boiling heat transfer enhancement employing an experimental study", *Int. J. Heat Mass Transf.*, **141**, pp. 974–980 (2019).
16. Ahmad, S., Ashraf, M., and Ali, K. "Nanofluid flow comprising gyrotactic microorganisms through a porous media", *JAFM*, **13**(5), pp. 1539–1549 (2020).
17. Khan, S.A. and Siddiqui, M.A. "Numerical studies on heat and fluid flow of nanofluid in a partially heated vertical annulus", *Heat Transfer*, **49**(3), pp. 1458–1490 (2020).
18. Irfan, M., Farooq, M.A., and Iqra, T. "A new computational technique design for EMHD nanofluid flow over a variable thickness surface with variable liquid characteristics", *Front. Phys.*, **8**(66), 66(1–14) (2020). DOI: 10.3389/fphy.2020.00066
19. Turkyilmazoglu, M. "Multiple analytic solutions of heat and mass transfer of magnetohydrodynamic slip

flow for two types of viscoelastic fluids over a stretching surface", *J. Heat Transfer*, **134**(7), 071701(1–9) (2012). DOI: 10.1115/1.4006165

20. Khan, Y. "Magnetohydrodynamic flow of linear viscoelastic fluid model above a shrinking/stretching sheet: A series solution", *Sci. Iran.*, **24**(5), pp. 2466–2472 (2017).

21. Kumar, R., Sood, S., Sheikholeslami, M., et al. "Nonlinear thermal radiation and cubic autocatalysis chemical reaction effects on the flow of stretched nanofluid under rotational oscillations", *J. Colloid Interface Sci.*, **505**, pp. 253–265 (2017).

22. Irfan, M., Farooq, M.A., and Iqra, T. "Magnetohydrodynamic free stream and heat transfer of nanofluid flow over an exponentially radiating stretching sheet with variable fluid properties", *Front. Phys.*, **7**(186), 186(1-11) (2019). DOI: 10.3389/fphy.2019.00186

23. Akhter, S., Ashraf, M., and Ali, K. "MHD flow and heat transfer analysis of micropolar fluid through a porous medium between two stretchable disks using quasi-linearization method", *Iran. J. Chem. Chem. Eng.*, **36**(4), pp. 155–169 (2017).

24. Akhter, S. and Ashraf, M. "Numerical study of flow and heat transfer in a porous medium between two stretchable disks using Quasi-linearization method", *Therm. Sci.*, **25**(2), pp. 989–1000 (2021). DOI: 10.2298/TSCI180801163A

25. Turkyilmazoglu, M. "Stretching/shrinking longitudinal fins of rectangular profile and heat transfer", *Energy Convers. Manag.*, **91**, pp. 199–203 (2015).

26. Turkyilmazoglu, M. "Latitudinally deforming rotating sphere", *Appl. Math. Model.*, **71**, pp. 1–11 (2019).

27. Farooq, M., Salahuddin, A., Razzaq, M., et al. "Computational analysis for unsteady and steady magnetohydrodynamic radiating nano fluid flow past a slippery stretching sheet immersed in a permeable medium", *Sci. Iran.*, **27**(6), pp. 3454–3466 (2020). DOI: 10.24200/SCI.2020.53055.3039

28. Kuznetsov, A.V. "The onset of nanofluid bioconvection in a suspension containing both nanoparticles and gyrotactic microorganisms", *Int. Commun. Heat Mass Transf.*, **37**(10), pp. 1421–1425 (2010).

29. Kuznetsov, A.V. "Nanofluid bioconvection in water-based suspensions containing nanoparticles and oxytactic microorganism: Oscillatory instability", *Nanoscale Res. Lett.*, **6**, 100(1–13) (2011). DOI: 10.1186/1556-276X-6-100

30. Khan, W.A., Rashad, A.M., Abdou, M.M.M., et al. "Natural bioconvection flow of a nanofluid containing gyrotactic microorganisms about a truncated cone", *European J. Mech. - B/Fluids*, **75**, pp. 133–142 (2019).

31. Hayat, T., Waqas, M., Shehzad, S.A., et al. "Mixed convection flow of viscoelastic nanofluid by a cylinder with variable thermal conductivity and heat source/sink", *Int. J. Numer. Method H.*, **26**(1), pp. 214–234 (2016).

32. Mehryan, S.A.M., Kashkooli, F.M., Soltani, M., et al. "Fluid flow and heat transfer analysis of a nanofluid containing motile gyrotactic micro-organisms passing a nonlinear stretching vertical sheet in the presence of a non-uniform, magnetic field numerical approach", *PLOS*, **11**(6), e0157598(1–32) (2016). DOI: 10.1371/journal.pone.0157598

33. Akbar, N.S. "Bioconvection peristaltic flow in an asymmetric channel filled by nanofluid containing gyrotactic microorganism", *Int. J. Numer. Method H.*, **25**(2), pp. 214–224 (2015).

34. Atif, S.M., Hussain, S., and Sagheer, M. "Magnetohydrodynamic stratified bioconvective flow of micropolar nano fluid due to gyrotactic microorganisms", *AIP Adv.*, **9**(2), 025208(1–17) (2019). DOI: 10.1063/1.5085742

35. Zuhra, S., Khan, N.S., Shah, S., et al. "Simulation of bioconvection in the suspension of second grade nanofluid containing nanoparticles and gyrotactic microorganisms", *AIP Adv.*, **10**(8), 105210(1–24) (2018). DOI: 10.1063/1.5054679

36. Atif, S., Hussain, S., and Sagheer, M. "Effect of thermal radiation on MHD micropolar Carreau nanofluid with viscous dissipation, Joule heating, and internal heating", *Sci. Iran.*, **26**(6), pp. 3875–3888 (2019).

37. Nawaz, M. "Numerical study of hydrothermal characteristics in nano fluid using KKL model with Brownian motion", *Sci. Iran.*, **26**(3), pp. 1931–1943 (2019).

38. Ferdows, M., Zaimi, K., Rashad, A.M., et al. "MHD bioconvection flow and heat transfer of nanofluid through an exponentially stretchable sheet", *Symmetry*, **12**(5), 692(1–18) (2020). DOI: 10.3390/sym12050692

39. Shakiba, A. and Rahimi, A.B. "Role of movement of the walls with time-dependent velocity on flow and mixed convection in vertical cylindrical annulus with suction/injection", *Sci. Iran.*, 21932(1–24) (2020). (In Press) DOI: 10.24200/SCI.2020.54784.3917

40. Ahmed, A., Khan, M., Ahmed, J., et al. "Mixed convection in unsteady stagnation point flow of Maxwell fluid subject to modified Fourier's law", *Arab. J. Sci. Eng.*, **45**, pp. 9439–9447 (2020).

41. Aman, F., Hafizah, W.N., Khazim, W.M., et al. "Mixed convection flow of a nanofluid containing gyrotactic microorganisms over a stretching/shrinking sheet in the presence of magnetic field", *IOP Conf. Series: Journal of Physics: Conf. Series*, **890**, 012027(1–8) (2017). DOI: 10.1088/1742-6596/890/1/012027

42. Ahmad, S., Ashraf, M., and Ali, K. "Heat and mass transfer flow of gyrotactic microorganisms and nanoparticles through a porous medium", *Int. J. Heat and Technol.*, **32**(2), pp. 395–402 (2020).

43. Sheikholeslami, M. and Rokni, H.B. "Effect of melting heat transfer on nanofluid flow in the presence of a

magnetic field using the Buongiorno Model", *Chin. J. Phys.*, **55**(4), pp. 1115–1126 (2017).

44. Wahid, N.S., Hafidzuddin, M.E.H., Arifin, N.M., et al. "Magnetohydrodynamic (MHD) slip Darcy flow of viscoelastic fluid over a stretching sheet and heat transfer with thermal radiation and viscous dissipation", *CFD Lett.*, **12**(1), pp. 1–12 (2020).
45. Wahid, N.S., Hafidzuddin, M.E.H., Arifin, N.M., et al. "Exact analytical solution for MHD flow and heat transfer of Jeffrey fluid over a stretching sheet with viscous dissipation", *JMEST*, **6**(12), pp. 49–53 (2019).
46. Wahid, N.S., Arifin, N.M., Turkyilmazoglu, M., et al. "MHD Hybrid Cu-Al_2O_3/ Water nanofluid flow with thermal radiation and partial slip past a permeable stretching surface: analytical solution", *J. Nano R.*, **64**, pp. 75–91 (2020).
47. Turkyilmazoglu, M. "The analytical solution of mixed convection heat transfer and fluid flow of a MHD viscoelastic fluid over a permeable stretching surface", *Int. J. Mech. Sci.*, **77**, pp. 263–268 (2013).
48. Khan, S.U., Shehzad, S.A., Rauf, A., et al. "Mixed convection flow of couple stress nanofluid over oscillatory stretching sheet with heat absorption/generation effects", *Results Phys.*, **8**, pp. 1223–1231 (2018).
49. Lund, L.A., Omar, Z., Khan, I., et al. "Convective effect on magnetohydrodynamic (MHD) stagnation point flow of Casson fluid overa vertical exponentially stretching/shrinking surface: triple solutions", *Symmetry*, **12**(8), 1238(1–16) (2020). DOI: 10.3390/sym12081238
50. Mustafa, I., Abbas, Z., Arif, A., et al. "Stability analysis for multiple solutions of boundary layer flow towards a shrinking sheet: analytical solution by using least square method", *Phys. A Stat. Mech. Its Appl.*, **540**, 123028(1–12) (2020). DOI: 10.1016/j.physa.2019.123028

Biographies

Shaheen Akhter is a PhD Scholar under the supervision of Professor Dr. Muhammad Ashraf in the Centre for Advanced Studies in Pure and Applied Mathematics, Bahauddin Zakariya University, Multan, Pakistan. She is also a Lecturer at COMSATS University Islamabad (Sahiwal Campus), Pakistan.

Muhammad Ashraf is currently a Professor in the Centre for Advanced Studies in Pure and Applied Mathematics, Bahauddin Zakariya University, Multan, Pakistan. He has a teaching experience of more than 25 years. His research interests include flow, heat and mass transfer analysis of micropolar, Casson, Nano, hybrid-Nano, and dusty fluids using numerical methods. Moreover, his PhD students are working on the topics such as flow through Darcy-Forchheimer medium and fluid flows contacting gyrotactic microorganisms.